



# N, S co-doped biomass derived carbon with sheet-like microstructures for supercapacitors

Linlin Ji <sup>a</sup>, Bin Wang <sup>a, b, \*\*, \*</sup>, Yanling Yu <sup>c</sup>, Nuoxin Wang <sup>d</sup>, Jinbao Zhao <sup>a, \*</sup>

<sup>a</sup> State-Province Joint Engineering Laboratory of Power Source Technology for New Energy Vehicle, Engineering Research Center of Electrochemical Technology, Ministry of Education, College of Chemistry and Chemical Engineering, Xiamen University, Xiamen, 361005, Fujian, China

<sup>b</sup> School of Materials Science and Engineering, Southwest Jiaotong University, Chengdu, 610031, China

<sup>c</sup> School of Chemistry and Chemistry Engineering, Harbin Institute of Technology, Harbin, 150001, PR China

<sup>d</sup> Guizhou Center for Translational Medicine, Affiliated Hospital of Zunyi Medical University, Zunyi, 563000, PR China

## ARTICLE INFO

### Article history:

Received 12 October 2019

Accepted 20 November 2019

Available online 21 November 2019

### Keywords:

Biomass derived carbon

Sheet-like microstructure

N

S co-doping

Supercapacitors

## ABSTRACT

In this study, N, S co-doped bamboo fiber derived carbon has been prepared when  $K_3Fe(CN)_6$  and thiourea are selected as graphitization catalysis and dopant, respectively. The derived carbon possesses a large  $S_{BET}$ , suitable graphitization degree, excellent conductivity and wettability of electrolyte, and particularly, it exhibits a unique sheet-like microstructure derived from the layer stripping of gas produced by thiourea pyrolysis, and these microstructure features are very beneficial for energy storage. Typically, the derived carbon displays a high specific capacitance of 328 F/g and an acceptable rate capability of 61.3% at 15 A g<sup>-1</sup> in three-electrode systems. Meanwhile, the derived carbon-based coin-type symmetric supercapacitors are assembled in an aqueous electrolyte and an ionic liquid electrolyte, respectively, and they all show a considerable synergetic energy-power output performance (21.2 Wh kg<sup>-1</sup> at 454 W kg<sup>-1</sup> in aqueous electrolyte, and 61.6 Wh kg<sup>-1</sup> at 300 W kg<sup>-1</sup> in ionic liquid electrolyte), indicating the potential application of the derived carbon in supercapacitors.

© 2019 Elsevier Ltd. All rights reserved.

## 1. Introduction

In recent years, many researchers are committed to developing biomass-derived carbons (BDCs), and they apply BDCs to supercapacitors (SCs) due to their rich sources, unique microstructures, low costs and other outstanding advantages [1]. However, with the development of the research, the disadvantages of BDCs are gradually exposed. The main disadvantages of BDCs are as follows: i) a structure dominated by only micropores reduces the accessible surface area of electrolyte, although these microporous can provide a large specific surface area [2,3]; ii) poor graphitization results in unsatisfactory rate performance [4,5]; iii) the natural hydrophobic surface causes a low specific capacity [6,7].

In responses to the above disadvantages of BDCs, some

researchers have made relevant efforts. To improve the microscopic pore structure of BDCs, Li et al. [8] and Cheng et al. [9] prepared the porous BDC based on the hollow structure of willow catkin and “shell @ pearls” structure of squid inks, respectively, and they all obtained BDC with a considerable mesoporous structure. To improve the natural hydrophobic surface of BDCs, heteroatom doped BDCs were also prepared by Niu et al. [10] and Zhang et al. [11], and they are based on the hydroxyapatites component rich in cattle bones and alginate component rich in porphyrin, respectively. Apparently, in the current study, the researcher's ideas are focused on using biomass rich in special structures or components as the carbon sources. Unfortunately, these special biomasses are difficult to collect due to seasonal and geographical influences. Therefore, the above research ideas are obviously unsatisfactory.

Doping heteroatoms has proven to be an effective method for improving the surface wettability of carbon materials. The most common one is to dope N atoms into the carbon matrix. Studies have shown that N-doping not only makes the surface of carbon material wettable, but also improves its conductivity, which are based on the fact that N atoms have different electronegativity from adjacent C atoms [12,13]. Compared with N atoms, S atoms have larger size and higher electrochemical activity [14]. If doping S

\* Corresponding author.

\*\* Corresponding author. State Key Lab of Physical Chemistry of Solid Surfaces, College of Chemistry and Chemical Engineering, Collaborative Innovation Center of Chemistry for Energy Materials, State-Province Joint Engineering Laboratory of Power Source Technology for New Energy Vehicle, Xiamen University, Xiamen, 361005, Fujian, China.

E-mail addresses: [jeasonbin@163.com](mailto:jeasonbin@163.com) (B. Wang), [jbzha@xmu.edu.cn](mailto:jbzha@xmu.edu.cn) (J. Zhao).

atoms into the carbon matrix, the S atom functional groups will destroy the electron balance density of the carbon surface and bring about different bond lengths and angles [15]. Therefore, S-doping ensures a more wettable carbon material surface, meanwhile, introduces a considerable electrochemical reversible reaction, further providing an additional Faraday capacitance. Recently, dual-doped manner (such as B/N, N/S) has attracted the attention of researchers. For example, both Gopalsamy et al. [16] and Zhang et al. [17] compared the electrochemical performance of N, S co-doped and single-doped (N or S) graphene, and the results showed that the former is significantly better than the latter. These phenomena are based on that dual-doping can comprehensively enhance the electrochemical performance of carbon materials due to the synergetic effect [18]. Hence, heteroatom co-doped carbon has great potential in electrochemical energy storage.

Traditionally, the highly graphitized BDCs can be obtained at a carbonization temperature greater than 2500 °C, however, this process needs high energy consumption and can lead to poor porosity of BDCs [19]. Fortunately, the carbonization temperature can be significantly reduced by graphitization catalysts (e.g., Fe, Co, Ni) [20,21]. The formation-decomposition intermediate theory has explained this catalytic process as follows: the d-orbitals of these graphitization catalysts will accept electrons of carbon to form metal carbide intermediate, and the intermediate will decompose as the temperature increases, meanwhile, the amorphous carbon will be converted into the layered graphitic carbon [22,23]. Highly graphitized BDCs have been prepared by the catalytic method [24], and recently, researchers hope that the graphitization catalyst can also act as an activator or dopant when preparing BDCs. For example, Gong et al. prepared BDCs with a high graphitization degree and large specific surface area when  $K_2FeO_4$  is used as a catalyst and an activator [25]. The above research concept is expected to further reduce the cost of BDC and is worthy of development.

Recently, the application of 2-dimensional (2D) carbon materials (e.g., graphene, sheet-like carbon [26–29]) to electrochemical energy storage has attracted wide attention from researchers. This is based on the fact that the 2D carbon possesses an essential advantage of significantly shortening the ion transport length [30]. The short ion transport length results in a small ion transport time (ion transport time can be obtained by the following formula:  $\tau = l^2/d$ , where  $\tau$ ,  $l$  and  $d$  are ion transport time, length and coefficient, respectively), further enabling the carbon material to achieve high power [31]. The latest, 2D biomass-derived carbon (BDC) has been prepared and applied to SCs, all of which exhibit excellent electrochemical performance [32,33]. Based on the above research progresses, in this study, we use bamboo fiber (BF) as the carbon source, which has more practical research significance than special biomass due to its huge reserves. Simultaneously, the study selected potassium ferricyanide ( $K_3Fe(CN)_6$ ) and thiourea as graphitization catalyst and dopant, respectively. The study was conducted based on the following facts: i) the graphitization catalyst  $K_3Fe(CN)_6$  can participate in the preparation of BDC as a co-activator (based on its K species). ii) The hydrophobic surface of BDC can be significantly improved by N, S co-doping. iii) The sheet-like structure can be formed by layer stripping of heteroatom-containing gas ( $NH_3$  and  $H_2S$ , derived from the pyrolysis of thiourea [34]). The microstructural characterization of target product corresponds to the protocol of this study: first, the target product possesses a large specific surface area and high conductivity; second, it exhibits a rich sheet-like structure; third, it also exhibits good wettability to the electrolyte. Consequently, these advantages of the target product give it outstanding capacitive performance, and this approach will bring hope to the practical application of BDCs in SCs.

## 2. Experimental

### 2.1. Sample preparation

The original BF used was collected from Fujian province (Southeastern China), cut into small pieces, washed by deionized water (4 g for 100 mL) at 90 °C for 4 h to remove the dirt, and then vacuum dried before use. The preparation process of target product N, S co-doped graphitization BF derived carbon (NSGBC) was as following: first, a certain amount of cleanly BF was pyrolyzed at 400 °C in Ar atmosphere for 2 h, and obtained the pre-carbonized BF derived carbon (PBC); second, PBC, KOH,  $K_3Fe(CN)_6$  and thiourea were mixed at mass ratio of 1:2:1:0.2 and fully milled in a mortar, and then the mixture was carbonized at 800 °C (5 °C/min) for 4 h under Ar atmosphere; finally, the resulting product was washed by 1 M HCl and water, and dried at 80 °C for 12 h. For comparison, KOH activated BF derived carbon (BC, without  $K_3Fe(CN)_6$  and thiourea), activated-graphitized BF derived carbon (GBC, without thiourea), N, S co-doped BF derived carbon (NSBC, without  $K_3Fe(CN)_6$ ), graphitized BF derived carbon (GC, without KOH and thiourea) and directly carbonized BF (BFC, without KOH,  $K_3Fe(CN)_6$  and thiourea) were also prepared by the similar method.

### 2.2. Characterizations

The morphology and element distribution of samples were observed by scanning electron microscope (HITACHI, S-4800, SEM) and transmission electron microscopy (TECNAI F30, TEM), respectively. The graphitization degree and defects derived from heteroatom of samples were measured by Raman spectroscopy (HORIBA Xplora) and X-ray diffraction spectrometer (Rigaku miniflex 600, XRD). Meanwhile, the conductivity was tested by a semiconductor resistivity of the powder tester (JGR ST-2722). Specific surface area was obtained by  $N_2$  adsorption/desorption method at liquid nitrogen temperature (77 K) on a Micromeritics ASAP-2020 analyzer. The content and valence states of heteroatoms were analyzed by X-ray photoelectron spectroscopy (XPS, performed on PHI Quantum 5000 equipped with an Al K $\alpha$  radiation). The electrolyte wettability of samples were confirmed by a commercial drop shape analysis system (Powereach JC2000C1, Shanghai Zhongchen Digital Technique Equipment Co. Ltd., China).

### 2.3. Electrochemical tests

For electrochemical tests, the working electrode was prepared as following: first, the active material, acetylene blank and polytetrafluoroethylene (PTFE) were mixed at a mass ratio of 90:5:5, and 50  $\mu$ L ethanol was added to the mixture and thoroughly ground to obtain a slurry; subsequently, the slurry was coated onto the stainless mesh (1  $\times$  1 cm<sup>2</sup>); finally, the electrode was dried at 80 °C for 12 h and compressed at 5 MPa for 5 min. The electrochemical performance of samples was measured by an electrochemical workstation (CHI 660D, Shanghai Chenhua, China) in a variety of electrolytes. The electrochemical performance of each sample was first investigated by a three-electrode system in 1 M  $H_2SO_4$  with saturated calomel electrode and platinum foil as the reference and counter electrode, respectively. And then, the performance of the NSGBC-based symmetric supercapacitors was investigated by a two-electrode cell device (CR2032 coin-type cell, a filter paper as the separator, the electrode was still prepared by the above method, just a nickel foam with a diameter of 12 mm as the current collector) in a neat ionic liquid 1-ethyl-3-methylimidazolium bis(trifluoromethylsulfanyl) imide (EMIM TFSI), 1 M  $Na_2SO_4$  and 1 M  $H_2SO_4$  at different voltage windows.

Cyclic voltammetry (CV), galvanostatic charge/discharge (GCD)

and electrochemical impedance spectroscopy (EIS), were carried out in the frequency range from  $10^{-2}$ – $10^5$  Hz. The mass specific capacitance ( $C$ ,  $F g^{-1}$ ) of single electrode and symmetric supercapacitors based on GCD curves was evaluated according to equation  $C = It/m\Delta V$ , where  $I$ ,  $t$  and  $\Delta V$  are the discharge current (A), discharge time (s) and working voltage window (V), respectively. The  $m$  is the mass of active material on single working electrode and total mass of NSGBC on both working electrode in three-electrode system and symmetric device, respectively. The energy density ( $E$ ,  $Wh kg^{-1}$ ) and power density ( $P$ ,  $W kg^{-1}$ ) of symmetric device were calculated by following equations based on GCD tests:  $E = C(\Delta V)^2/2$  and  $P = E/\Delta t$ , where  $C$ ,  $\Delta V$  and  $\Delta t$  are specific capacitance, working voltage window and discharge time of symmetric device, respectively [35].

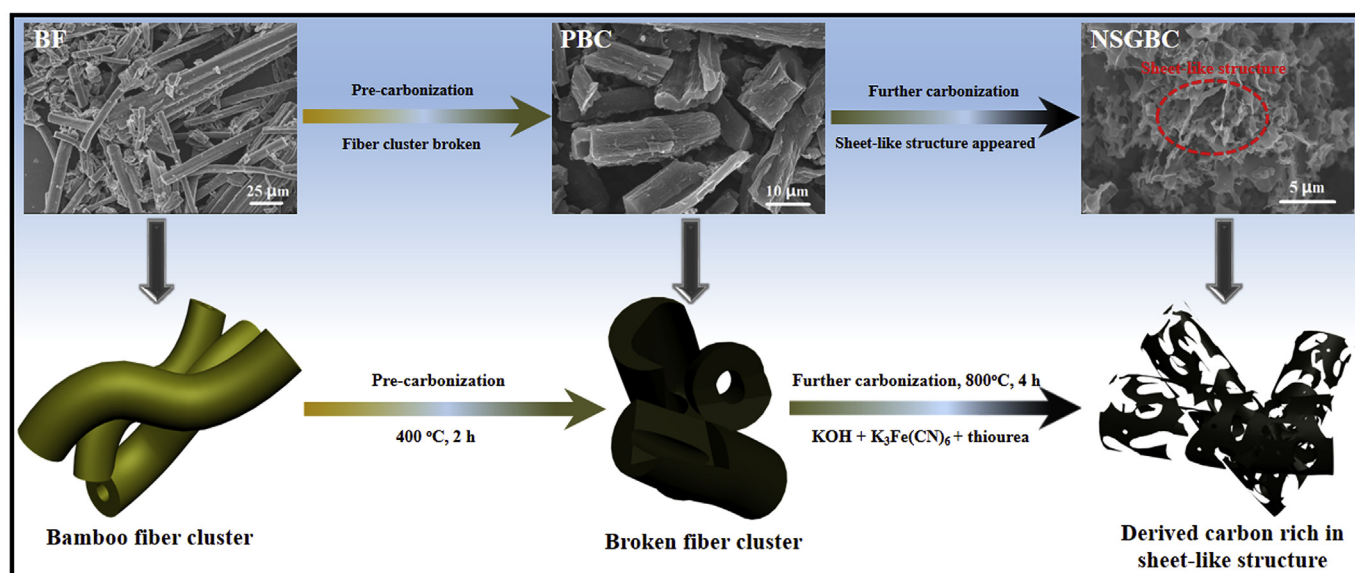
### 3. Results and discussion

#### 3.1. Microstructure characterization

**Scheme 1** illustrates the preparation process of target sample NSGBC. Briefly, the fiber cluster structure of BF was destroyed via direct pre-carbonization at  $400^\circ C$ , thereby, a pre-carbonization derived carbon PBC was obtained. And then, the target sample NSGBC (rich in sheet-like structure) was obtained by further carbonizing PBC with KOH,  $K_3Fe(CN)_6$  and thiourea, and the sheet-like structure may be result from the layer peeling of the gas generated when thiourea is pyrolyzed. In order to prove the speculation, BF derived carbon treated with KOH (BC) and KOH +  $K_3Fe(CN)_6$  (GBC), respectively, were also prepared, and their micromorphology are shown in **Fig. 1**. Intuitively, BC (**Fig. 1a**) exhibits a rich macroporous structure and highly 3-D interconnected frameworks originating from the KOH activation. GBC (**Fig. 1b**) possesses a richer 3-D interconnected framework compared with BC, which is probably due to the auxiliary activation of  $K_3Fe(CN)_6$ . The auxiliary activation effect has been demonstrated by GC (PBC is treated only with  $K_3Fe(CN)_6$ ) and BFC (PBC is directly carbonized), and the SEM images and nitrogen adsorption/desorption isotherms of them are shown in **Figs. S1 and S3**, respectively. Apparently, the broken fiber cluster structure of BFC is destroyed by the treatment of  $K_3Fe(CN)_6$ , and the specific surface area ( $S_{BET}$ ) of GC is much

larger than that of BFC (the  $S_{BET}$  of GC and BFC are  $760$  and  $0.7 m^2 g^{-1}$ , respectively). These phenomena indicate that  $K_3Fe(CN)_6$  possesses an additional activation in the process of further carbonizing PBC, which is attributed to the K species of  $K_3Fe(CN)_6$ . Moreover, it is noteworthy that the sheet-like structure has not yet appeared under the preparation conditions of GBC. However, the special structure appeared when the thiourea was added (NSGBC, **Fig. 1c**), indicating that the formation of sheet-like structure is dependent on the layer stripping effect of the gas produced by the pyrolysis of thiourea. The highly-developed microporous structure of NSGBC is revealed by its TEM image (**Fig. S2a**), which will result in a large  $S_{BET}$ . Meanwhile, the HRTEM image of NSGBC (**Fig. 1d**) displays that the well-graphitized walls are arranged in an orderly direction, which can be well defined as (002) lattice fringes, and this definition is confirmed by the selected area electron diffraction pattern (SAED pattern, **Fig. S2b**). It suggests that  $K_3Fe(CN)_6$  can promote the graphitization of BF derived carbon. Moreover, the element distribution of C, N, O and S in NSGBC are shown in **Fig. 1e–i**. The existence and uniform distribution of heteroatoms N and S are revealed, suggesting that the N and S atoms are successfully incorporated into the derived carbon matrix.

The graphitization degree and defects of samples were confirmed by Raman spectra, and the results are shown in **Fig. 2a**. Generally, all spectra can be fitted into four peaks centered at  $\sim 1251$ ,  $\sim 1359$ ,  $\sim 1519$  and  $\sim 1609 cm^{-1}$ , which can be defined to the I, D, D' and G bands, respectively [36]. The I band, is originated from impurities or heteroatoms (for NSGBC, it is originated from the N, O and S; for BC and GBC, is originated from the N and O); the D band, is attributed to the disorder induced by the  $sp^3$  defect sites on the graphitic plane; the D' band, is derived from the defects in graphene layer stacking; the G band, is assigned to the stretching bond of  $sp^2$  hybridized carbon and can be observed in all BDC [37]. Herein, the I band content of NSGBC is meaningfully larger than that of BC and GBC, which may be attributed to NSGBC having not only the most heteroatom type, but also the highest heteroatom content (further confirmed by XPS spectra). In addition, the graphitization degree of sample can be indicated by the area ratio of G and D bands, and denoted as  $I_G/I_D$ . Clearly, the  $I_G/I_D$  of GBC and NSGBC are much larger than that of BC due to the graphitization catalysis of  $K_3Fe(CN)_6$ . However, the  $I_G/I_D$  of NSGBC is dramatically



**Scheme 1.** Schematic illustrations of the preparation process of NSGBC.

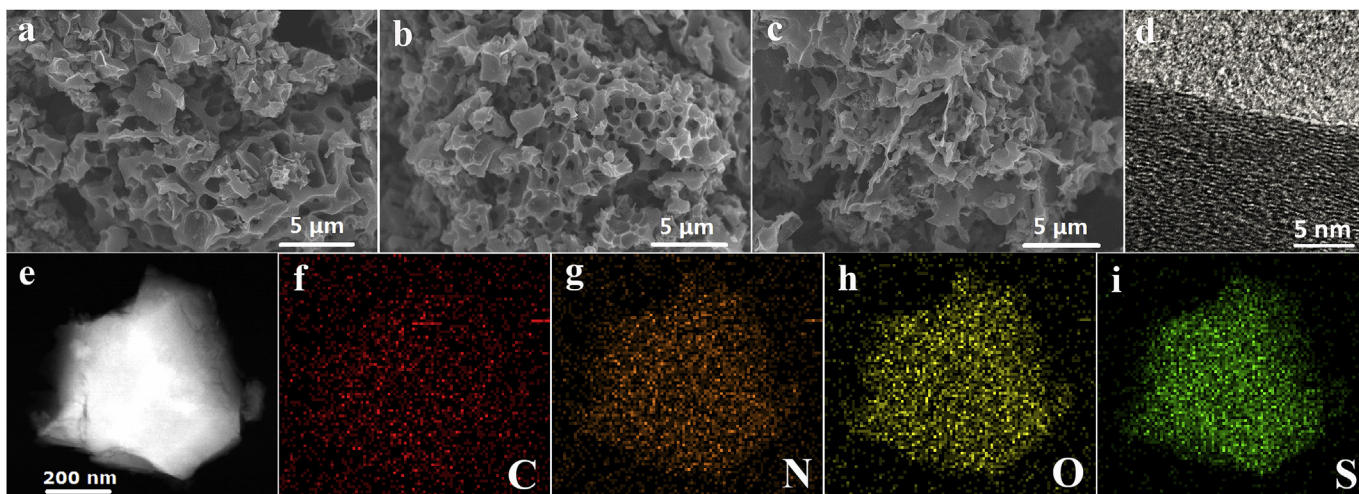


Fig. 1. SEM images of BC (a), GBC (b), NSGBC (c); HRTEM image of NSGBC (d); dark field TEM (e), C (f), N (g), O (h) and S (i) elemental mapping STEM images of NSGBC.

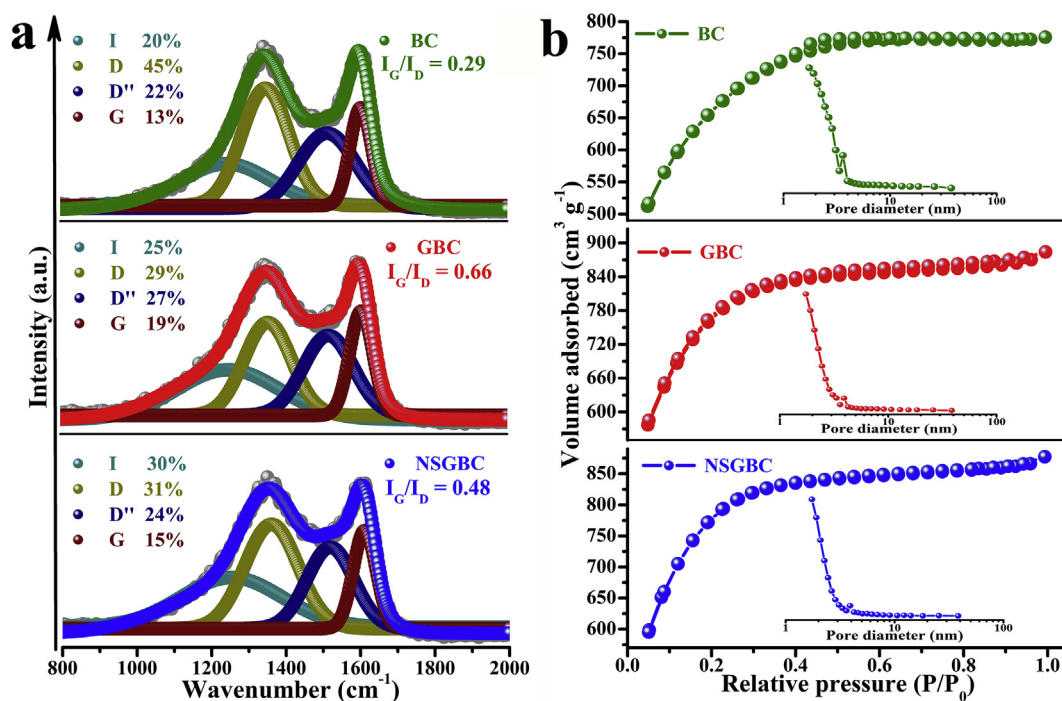


Fig. 2. Raman spectra (a) and nitrogen adsorption/desorption isotherm (b) of BC, GBC and NSGBC.

less than that of GBC, which is mainly attributed to a large number of defects caused by heteroatom doping.

To further confirm the effect of  $K_3Fe(CN)_6$  on the graphitization degree of samples, the XRD spectra of samples were performed (Fig. S4). In Fig. S4, two broad peaks were observed in BC and NSBC (their carbonization process does not add  $K_3Fe(CN)_6$ ), indicating their highly amorphous structure [19]. For GC (carbonization process adds  $K_3Fe(CN)_6$ ), its XRD pattern displays a sharp diffraction peak at  $26.5^\circ$ , which is attributed to the typical (002) plane of graphitic carbon, and indicating the highly graphitized structure [24]. Similar to GC, the sharp peak was also observed on the XRD patterns of GBC and NSGBC (their carbonization process adds  $K_3Fe(CN)_6$ ) due to their highly graphitized structure (consistent with the analysis results of TEM and Raman spectra). These phenomena further indicate that the  $K_3Fe(CN)_6$  can significantly

increase the graphitization degree of BF-derived carbon. Well-known, the conductivity of carbon material is closely related to its graphitization degree. The mean conductivity of samples was tested and the results are shown in Table S1. Clearly, the conductivity value of NSGBC ( $6.23 \text{ S cm}^{-1}$ ) is much larger than that of BC ( $0.56 \text{ S cm}^{-1}$ ) due to its excellent graphitization degree. Moreover, this value is greater than many biomass-derived carbons (hemp derived carbon,  $2.11\text{--}2.26 \text{ S cm}^{-1}$  [30], bamboo derived carbon,  $4.7 \text{ S cm}^{-1}$  [25]) and is even far superior to commercial activated carbon (Norit activated carbon,  $0.33 \text{ S cm}^{-1}$  [38]). In short, the above analysis reveals that  $K_3Fe(CN)_6$  can effectively increase the graphitization degree of NSGBC, thereby further improving the conductivity of NSGBC.

In order to reveal the abundant pore structure and high  $S_{BET}$  of samples, the nitrogen adsorption-desorption measurements were

**Table 1**  
Pore structure parameters and chemical compositions of BC, GBC and NSGBC.

Sample ID	Pore structure parameters				Element proportions			
	$S_{\text{BET}}^{\text{a}}$ ( $\text{m}^2 \text{g}^{-1}$ )	$V_{\text{T}}^{\text{b}}$ ( $\text{cm}^3 \text{g}^{-1}$ )	$V_{\text{mic}}/V_{\text{T}}^{\text{c}}$ (%)	$V_{\text{mes}}/V_{\text{T}}^{\text{d}}$ (%)	C/at. %	O/at. %	N/at. %	S/at. %
BC	2212	1.1998	79.5	17.6	86.9	12.2	0.9	—
GBC	2544	1.3674	84.0	11.8	89.3	8.6	2.1	—
NSGBC	2561	1.3570	84.7	10.7	88.5	6.1	3.2	2.2

<sup>a</sup> Specific surface area.

<sup>b</sup> The total pore volume.

<sup>c</sup> Percentage of microporous volume to total pore volume.

<sup>d</sup> Percentage of mesoporous volume to total pore volume.

performed, and the results are shown in Fig. 2b, summarized in Table 1. The same as the most carbon materials prepared by KOH activation method, the pattern of BC presents type-I isotherm, indicating the highly developed microporous structure [39,40]. Furthermore, a weak hysteresis loop was also observed at  $0.4 < P/P_0 < 0.7$ , indicating that BC possesses a certain mesoporous structures (derived from the organizational structure of BF). The  $S_{\text{BET}}$  of GBC and NSGBC are very close and greater than BC about 15.7%, which further proves the auxiliary activation of  $\text{K}_3\text{Fe}(\text{CN})_6$ . Meanwhile, the disappearance of the mesoporous structure derived from the BF's organizational structure (confirmed by pore size distribution, the inset of Fig. 2b) causes the  $V_{\text{T}}$  of GBC and NSGBC to also be meaningfully greater than that of BC. In general, GBC and NSGBC all exhibit high  $S_{\text{BET}}$  and large  $V_{\text{T}}$  due to the auxiliary activation of  $\text{K}_3\text{Fe}(\text{CN})_6$ , which will have a profound effect on their electrochemical performance.

The effect of different preparation conditions on the content and valence state of heteroatoms (N and S) were investigated by XPS spectra, and the results are shown in Fig. 3. The high-resolution C 1s spectra of BC and GBC can be deconvoluted into three peaks centered at  $\sim 284.4$ ,  $\sim 285.8$  and  $\sim 288.4$  eV, assigned to C–C/C=C in  $\text{sp}^2$ -hybridized domains, C–O/C–N and C=O/C=N, respectively [41]. For C 1s spectra of NSGBC, the peak of  $\sim 285.8$  eV is also

attributed to C–S owing to the introduction of a new heteroatom S. Notably, the C–C/C=C content of GBC and NSGBC is greater than that of BC, which is still due to the fact that  $\text{K}_3\text{Fe}(\text{CN})_6$  increases their graphitization degree. For N 1s orbit, BC can be fitted into three series ascribed to the pyridinic N (peak at  $\sim 398.9$  eV, N-1), pyrrolic N (peak at  $\sim 399.9$  eV, N-2) and quaternary N (peak at  $\sim 401.1$  eV, N-3), respectively. Among them, N-1 and N-2 possess excellent charge mobility due to their good electron-donor characteristics, which can further promote the electrochemical reactivity of carbon material surface [42]. N-3 is very beneficial to improve the conductivity of carbon material, owing to that the carbon atoms of the graphite crystallites are partially replaced by N atom [43,44]. The N content of GBC and NSGBC is much higher than that of BC due to the N species of  $\text{K}_3\text{Fe}(\text{CN})_6$  and dopant thiourea (Table 1), moreover, a new peak (centered at  $\sim 403.8$  eV) assigned to oxydic nitrogen (N-4) appears on their N 1s spectra [45], and it will significantly affect the wettability of the carbon material as a surface functional group. Consistent with experimental expectations, BC and GBC have no signal of S element, however, NSGBC exhibits an obvious S element signal, and the S 2p orbit can be fitted by three peaks at binding energies of  $\sim 163.5$  (S-1),  $\sim 164.8$  (S-2) and  $\sim 168.3$  (S-3). S-1 and S-2 are constrained by 1.3 eV binding energy separation, corresponding to the  $2\text{p}_{3/2}$  and  $2\text{p}_{1/2}$  of thiophene-like S

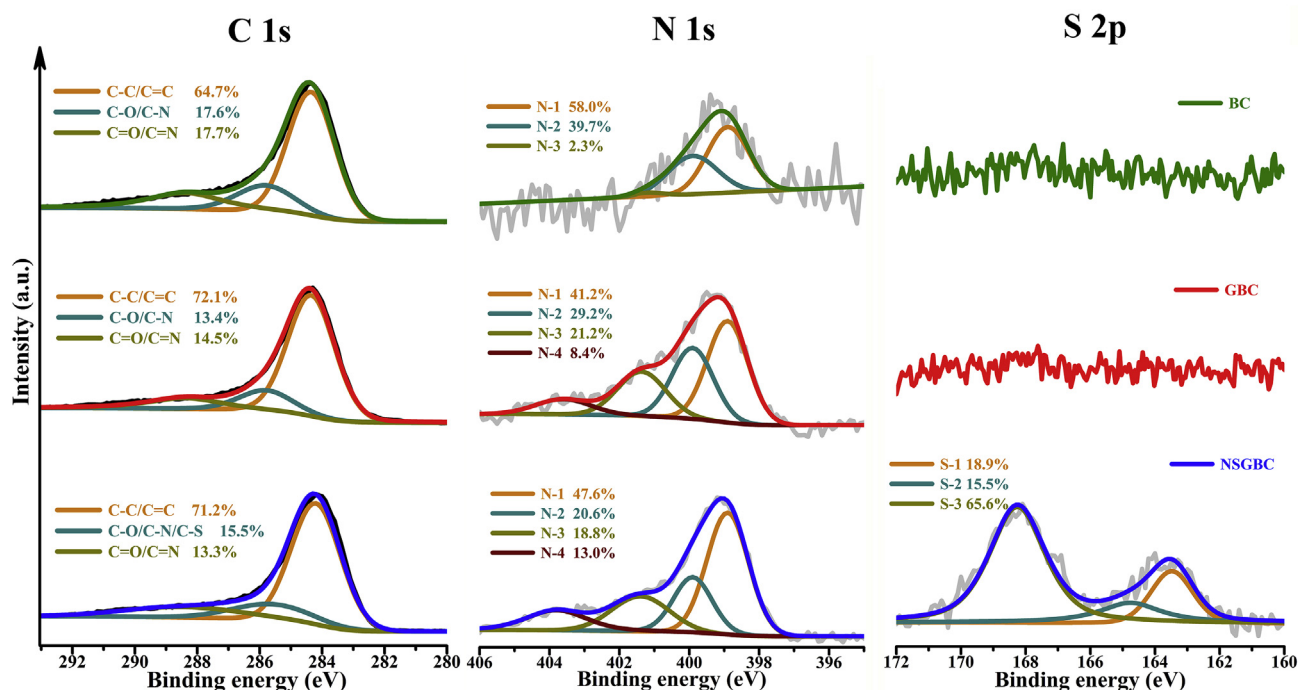


**Fig. 3.** High resolution C 1s, N 1s and S 2p XPS spectra of BC, GBC and NSGBC.

(C–S–C), respectively, due to their spin-orbit coupling; the last peaks (S-3) are appointed to the different oxidation states of C–SO<sub>x</sub>–C derived from the edge of the carbon scaffolds [46], and obviously, the content of S-3 is much higher than that of S-1 and S-2. Different with N element, S element will increase the electron density and polarization of the carbon surface when it incorporated into carbon matrix, and its oxygen-containing functional groups (e.g. sulfoxide and sulfone) will bring extra pseudo-capacitance [47]. Therefore, the high content of S-3 is advantageous for the specific capacitance of heteroatom-doped carbon. Of particular note, compared with NSBC (Table S2, PBC is treated by KOH and thiourea), NSGBC still presents a high heteroatom content (consistent with inference of Raman spectra), indicating that the addition of K<sub>3</sub>Fe(CN)<sub>6</sub> can promote heteroatom doping. Based on the fact that the contact angle of sample is meaningfully reduced as its heteroatom content increases (Fig. S7), the importance of the above phenomenon is self-evidence.

In brief summary, the finally product NSGBC exhibits a rich sheet-like structure derived from the layer stripping effect of the gas produced by the pyrolysis of thiourea, meanwhile, it also possesses a large S<sub>BET</sub>, suitable graphitization degree, excellent conductivity and high heteroatom doping ratio based on the addition of K<sub>3</sub>Fe(CN)<sub>6</sub>. Thence, it may present excellent electrochemical performance that is predictable.

### 3.2. Electrochemical behavior of samples for supercapacitors

The electrochemical behaviors of BC, GBC and NSGBC were first investigated by CV, GCD and EIS methods in 1 M H<sub>2</sub>SO<sub>4</sub> electrolyte under a three-electrode system, and the results are shown in Fig. 4. The CV curves of all samples (Fig. 4a) exhibit a typical quasi-rectangular shape, suggesting the ideal electrochemical double-

layer capacitance (EDLC) [48]. Moreover, NSGBC shows weakly broadened humps, which is mainly attributed to electrochemical reactions (Re. 1 ~ Re. 4) caused by heteroatom functional groups on its surface in the acidic electrolyte [48,49]. Further, NSGBC shows the maximum current response, which foreshadows its large specific capacitance. Corresponding to CV curves, the GCD curves of all samples (Fig. 4b) show an isosceles triangle shape with a slight deviation, which is still attributed to their dominant EDLC behavior. In the meantime, based on the discharge time of GCD test, the specific capacitance of BC, GBC and NSGBC are 195, 284 and 328 F/g, respectively, and these results are consistent with the prophecy of CV curves. In theory, the specific capacitance of carbon material should be proportional to its S<sub>BET</sub> [50], however, compared with BC, the increase in specific capacitance of NSGBC (~68.2%) is much larger than the increase in S<sub>BET</sub> (~15.8%, Table 1). This phenomenon is mainly owing to the following three points: i) the accessible surface area of NSGBC is increased because the heteroatom doping improves its surface wettability (Fig. S7); ii) the pseudocapacitance provided by the heteroatom functional groups [51]; iii) the electrochemical active site of NSGBC is completely exposed by sheet-like structure. For a better comparison, the specific capacitance of NSGBC and that in literature reports are summarized in Table 2. Intuitively, NSGBC is superior or close to many of the BDCs reported in the literature, even better than some graphene and MOF derived carbon.

The relationship between current density and specific capacitance of samples was investigated by GCD method at 1–15 A g<sup>-1</sup>, and the results are shown in Fig. 4c. For BC, a very dramatic potential drop (IR drop) appears on the GCD curve at 15 A g<sup>-1</sup> (Fig. S8a), and the GCD curve delivers a specific capacitance of 95 F/g, further, the capacitance retention is only 48.7% (compared with 195 F/g, at 1 A g<sup>-1</sup>). Fortunately, the IR drop of GBC and NSGBC

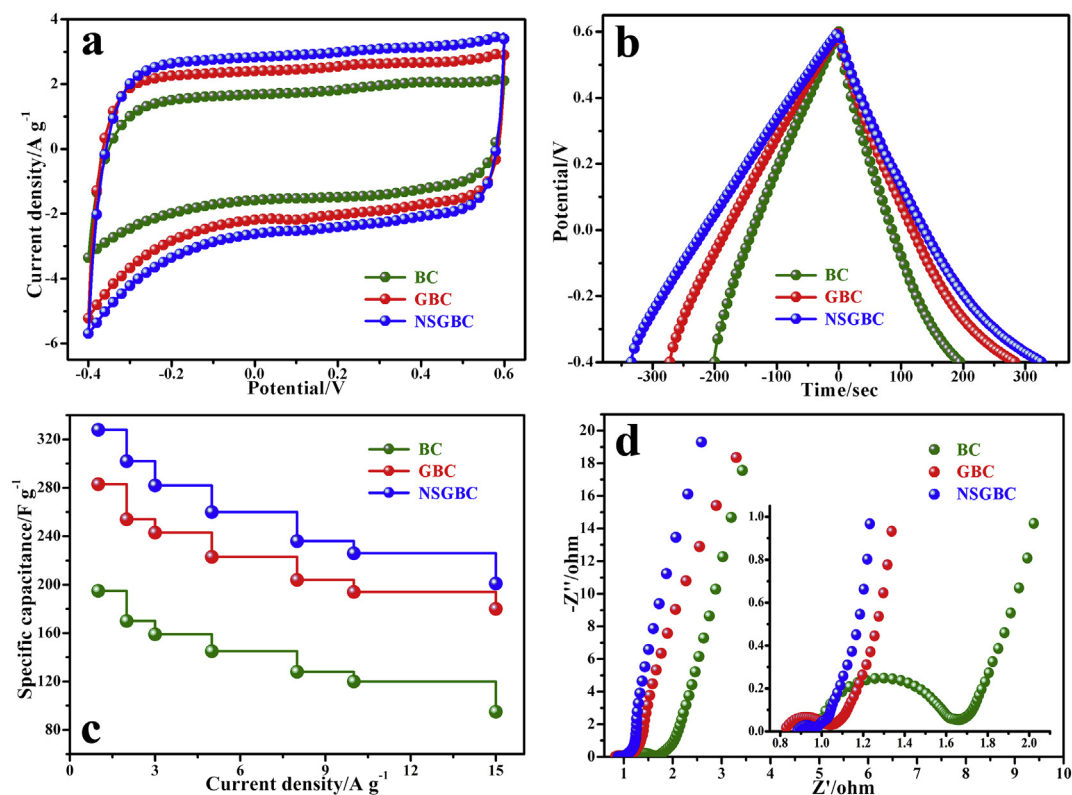


Fig. 4. CV (a, at a scan rate of 0.01 V s<sup>-1</sup>), GCD (b, at a current density of 1 A g<sup>-1</sup>) curves of BC, GBC and NSGBC; specific capacitance versus current density of BC, GBC and NSGBC (c); EIS curves of BC, GBC and NSGBC (d).

**Table 2**

Comparison of the specific capacitance for previously reported biomass-derived carbon and the star carbon materials.

Carbon type	Specific capacitance	Electrolyte	Ref.
Rice straw derived carbon	337 F/g (0.5 A/g)	6 M KOH	[3]
Bamboo derived carbon	222 F/g (0.5 A/g)	1 M H <sub>2</sub> SO <sub>4</sub>	[25]
Graphene	248 F/g (1.0 A/g)	6 M KOH	[52]
MOF derived carbon	233 F/g (5 mV/s)	1 M H <sub>2</sub> SO <sub>4</sub>	[53]
Catkins derived carbon	251 F/g (0.5 A/g)	1 M H <sub>2</sub> SO <sub>4</sub>	[54]
ZIF-8 derived carbon	219 F/g (5 mV/s)	1 M H <sub>2</sub> SO <sub>4</sub>	[55]
Cornstalk derived carbon	213 F/g (1 A/g)	6 M KOH	[56]
Nanofiber bridged carbon	261 F/g (2 mV/s)	1 M Na <sub>2</sub> SO <sub>4</sub>	[57]
Perilla derived carbon	270 F/g (0.5 A/g)	1 M Na <sub>2</sub> SO <sub>4</sub>	[58]
Carbon aerogel	283 F/g (1 A/g)	6 M KOH	[59]
Unconventional carbon	328 F/g (0.5 A/g)	6 M KOH	[60]
NSGBC	326 F/g (1 A/g)	1 M H <sub>2</sub> SO <sub>4</sub>	This work

(Figs. S8b and c) is much smaller than BC, and the capacitance retention of GBC and NSGBC is as high as 63.3% and 61.3%, respectively (specific capacitances are 180 and 201 F/g at 15 A g<sup>-1</sup>, respectively). These phenomena are consistent with the literature, and they suggest that IR drop is closely related to graphitization degree of material [61,62]. Moreover, the significant improvement in capacitance retention of GBC is also attributed to its wettability surface derived from heteroatom doping. For NSGBC, first, the wettability surface of sheet-like structure ensures that the electrolyte ion can diffuse into the highly-development microporous structure at a large current density, and second, the sheet-like structure can form a conductive network to further increase the conductivity of NSGBC. Hence, NSGBC also achieved excellent rate performance even though its graphitization degree was lower than that of GBC. The outstanding electrochemical performance of NSGBC was continually characterized by EIS method, and the

results are shown in Fig. 4d. The EIS plot of all samples contain a small semicircle at high frequency based on charge transfer resistance ( $R_{ct}$ ), a nearly diagonal line at medium frequency originated from Warburg impedance ( $R_w$ ), and a steep line at low frequency derived from ideal capacitive behavior [63]. Consistent with the foregoing analysis, NSGBC exhibits the smallest  $R_{ct}$  and  $R_w$  owing to its wettability surface of sheet-like structure. Furthermore, the intercept at the  $Z'$  axis of EIS plot represents the internal resistance ( $R_i$ ) caused by the active material resistance, electrolyte resistance and contact resistance between active material and current collector [64]. Herein,  $R_i$  directly reflects the intrinsic resistance of samples based on the same test conditions. As shown in the inset of Fig. 4d, the  $R_i$  of BC, GBC and NSGBC is 0.98, 0.82 and 0.88  $\Omega$ , respectively. Apparently, the  $R_i$  of samples is proportional to their graphitization degree.

Compared with acidic electrolyte, heteroatom-doped carbon generally exhibits a low specific capacitance in a neutral electrolyte, owing to the absence of the reversible electrochemical reaction (derived from the heteroatom functional groups) in a low H<sup>+</sup> concentration environment [65,66]. However, heteroatom-doped carbon exhibits a high over-potential in a neutral electrolyte, precisely due to the low H<sup>+</sup> concentration [67]. Real supercapacitors will present a large voltage window due to the above phenomenon, and further have a high energy density. Hence, many studies have assembled heteroatom-doped carbon-based symmetric supercapacitors with neutral electrolyte and tested their performance [68–70]. Herein, a real NSGBC-based coin-type symmetric supercapacitors is also assembled (active materials of positive and negative are both NSGBC, denoted as NSGBC//NSGBC-A) in 1 M Na<sub>2</sub>SO<sub>4</sub> aqueous electrolyte, and its capacitive performance test results are shown in Fig. 5. It can be seen that NSGBC//NSGBC-A can operate stably at a voltage window of 0–1.4 V to 0–1.8 V, and it

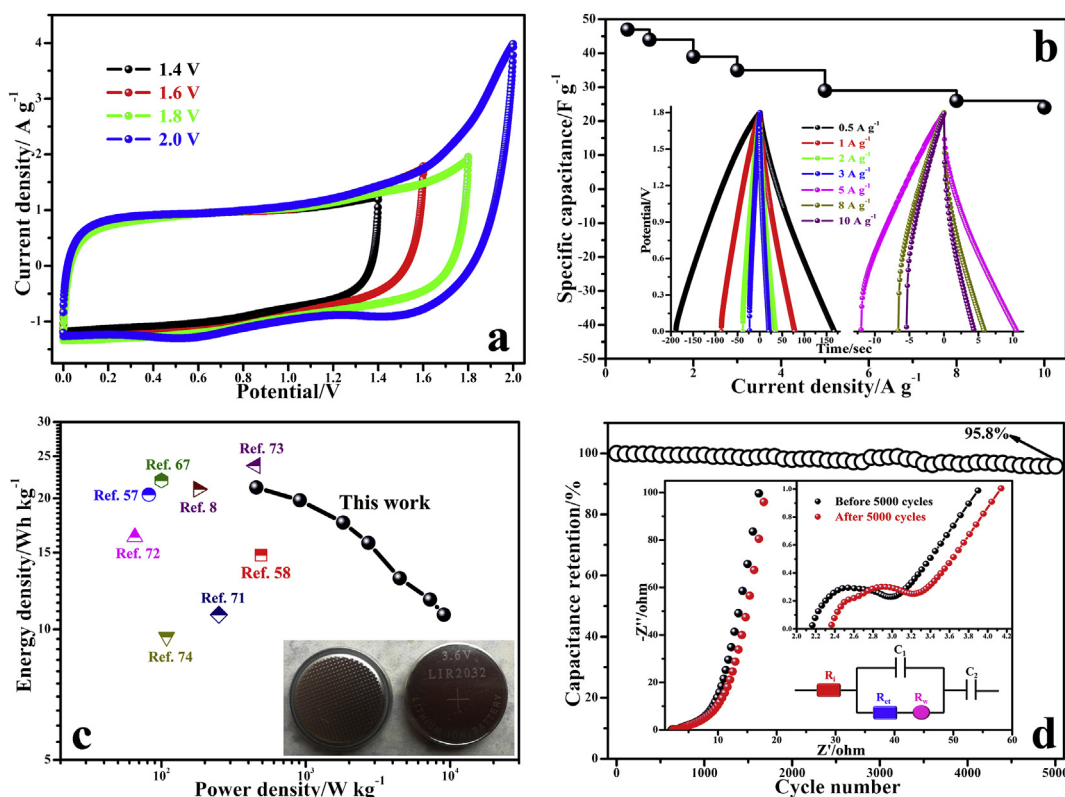


**Fig. 5.** CV curves (a, at a scan rate of 0.01 V s<sup>-1</sup>) of NSGBC//NSGBC-A at different potential windows; specific capacitance versus current density plots (b) and Ragone plot (c) of NSGBC//NSGBC-A at a potential window of 0–1.8 V; cycle stability of NSGBC//NSGBC-A at a current density of 3 A g<sup>-1</sup> (d, inset is a EIS curves of before and after 5000 cycles).

exhibits a significant polarization current until the voltage window increases to 0–2.0 V (Fig. 5a), implying that the suitable voltage window of NSGBC//NSGBC-A is 0–1.8 V, which is obviously greater than that of H<sub>2</sub>SO<sub>4</sub> electrolyte (for comparison, a NSGBC-based symmetric supercapacitors was assembled in H<sub>2</sub>SO<sub>4</sub> electrolyte and denoted as NSGBC//NSGBC-H, moreover, its suitable voltage window is 0–1.5 V, as shown in Fig. S10). Fig. 5b displays the GCD curves of NSGBC//NSGBC-A at a various current densities (0.5–10 A g<sup>-1</sup>) in 0–1.8 V. Consistent with literature report, whether it is specific capacitance or capacitance retention, NSGBC//NSGBC-A (specific capacitance is 47 F/g at 0.5 A g<sup>-1</sup>, capacitance retention is 51.1% at 10 A g<sup>-1</sup>) is less than NSGBC//NSGBC-H (specific capacitance is 47 F/g at 0.5 A g<sup>-1</sup>, capacitance retention is 61.3% at 10 A g<sup>-1</sup>, as shown in Fig. S11a).

The Ragone plots of NSGBC//NSGBC-A based on GCD tests at various current densities are displayed in Fig. 5c. It can be found that NSGBC//NSGBC-A exhibits the maximum energy density of 21.2 Wh kg<sup>-1</sup> with the power density of 454 W kg<sup>-1</sup>. Apparently, this value is greater than that of NSGBC//NSGBC-H (the maximum energy density is 18.2 Wh kg<sup>-1</sup> with the power density of 375 W kg<sup>-1</sup>, as shown in Fig. S11b). Meanwhile, the maximum energy density of NSGBC//NSGBC-A is highly competitive, compared with the already reported BDCs-based symmetric supercapacitors in Na<sub>2</sub>SO<sub>4</sub> electrolyte, such as perilla frutescens derived carbon (14.8 Wh kg<sup>-1</sup> at 490 W kg<sup>-1</sup>) [58], bacterial cellulose derived carbon (20.4 Wh kg<sup>-1</sup> at 81.8 W kg<sup>-1</sup>) [57], seaweed derived carbon (10.8 Wh kg<sup>-1</sup> at 250 W kg<sup>-1</sup>) [71], willow catkin derived carbon (21 Wh kg<sup>-1</sup> at 180 W kg<sup>-1</sup>) [8], fungus derived carbon (22 Wh kg<sup>-1</sup> at 100 W kg<sup>-1</sup>) [67], even also outperforms or equals to some star carbon materials based symmetric supercapacitors in Na<sub>2</sub>SO<sub>4</sub> electrolyte, e.g. heteroatoms doped graphene

(16.3 Wh kg<sup>-1</sup> at 65.4 W kg<sup>-1</sup> and 23.8 Wh kg<sup>-1</sup> at 448 W kg<sup>-1</sup>) [72,73] and mesoporous carbon (9.6 Wh kg<sup>-1</sup> at 108.5 W kg<sup>-1</sup>) [74]. Additionally, NSGBC//NSGBC-A displays outstanding cycling stability with 95.8% capacitance retention after repeating the GCD test 5000 cycles (at a current density of 3 A g<sup>-1</sup>). The inset of Fig. 5d compares the EIS plots before and after 5000 cycles, and similar to three-electrode systems, the plot consists of a short arc at high frequency, a nearly diagonal line at medium frequency and a nearly vertical line at low frequency. These EIS plots can be fitted by software of ZSimpWin based on an electrical equivalent circuit (as shown in the inset of Fig. 5d, where R<sub>i</sub>, C<sub>1</sub>, R<sub>ct</sub>, R<sub>w</sub> and C<sub>2</sub> are internal resistance, the EDLC, the charge transform resistance, the diffusion resistance and pseudocapacitance, respectively), and the fitted results are shown in Table S3. Intuitively, the R<sub>i</sub> has a slight increase, mainly due to the increase in contact resistance between NSGBC and current collector. However, R<sub>ct</sub> and R<sub>w</sub> remain basically unchanged after 5000 cycles, revealing that the unique microstructure and abundant heteroatoms functional groups of NSGBC are retained after cycling.

It is well known that the application of ionic liquids to carbon-based supercapacitors results in a large voltage window (0–2.5/3.0 V), which further increases the energy density of the device [75]. In order to further increase the energy density of NSGBC-based symmetric supercapacitors to be close to practical applications, a coin-type symmetric supercapacitors in a neat ionic liquid (EMIM TFSI, which can bring a large working voltage window) was assembled (denoted as NSGBC//NSGBC-I) and its capacitive performance has also been investigated (Fig. 6). According to the literature [25,76], carbon-based symmetric supercapacitors in EMIM TFSI ionic liquid are able to work stably at a working voltage window of 0–3 V. In this work, the electrochemical tests of NSGBC//

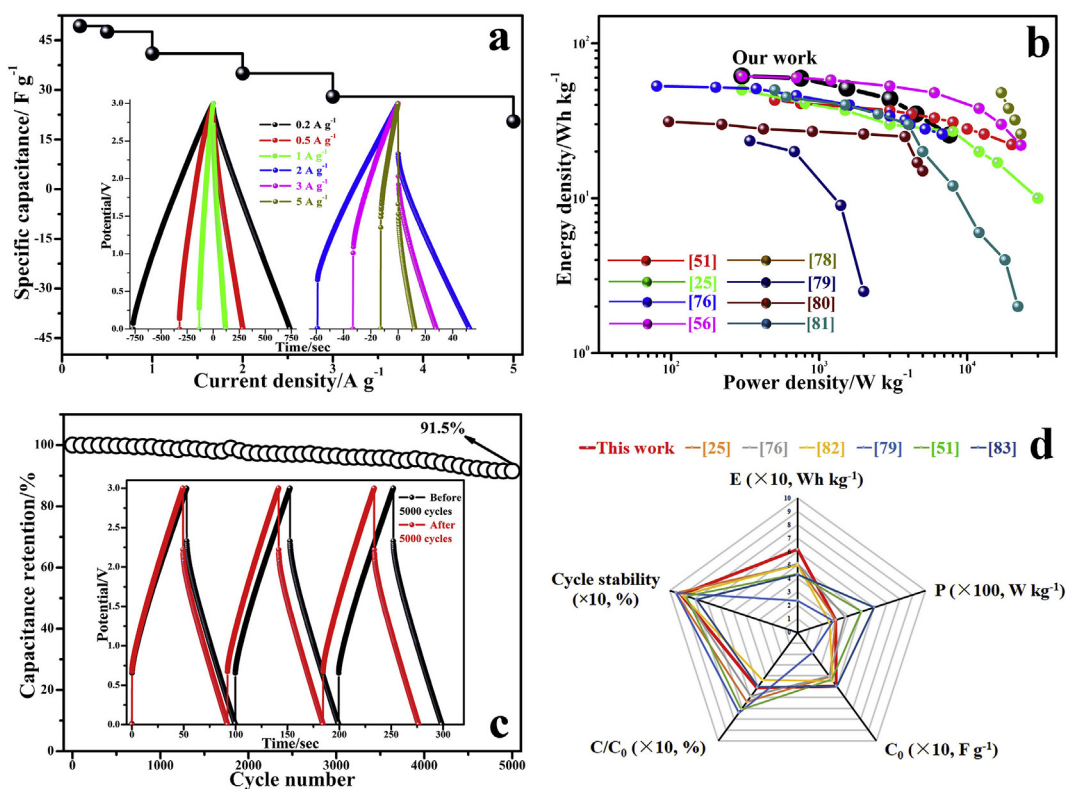


Fig. 6. Specific capacitance versus current density plots (a) and Ragone plot (b) of NSGBC//NSGBC-I; Cycle stability of NSGBC//NSGBC-I at a current density of 2 A g<sup>-1</sup> (c, inset is GCD curves of before and after 5000 cycles); Comparison of electrochemical performances of NSGBC//NSGBC-I with those of previously reported carbon materials in ionic liquid electrolyte (d).

NSGBC-I were also carried out at 0–3 V and first conducted a CV test (Fig. S14). The shape of NSGBC//NSGBC-I CV curve is still close to the rectangle, indicating the ideal EDLC behavior. Corresponding to CV curve, the GCD curves of NSGBC//NSGBC-I also exhibit an isosceles triangle-like shape (as shown in the inset of Fig. 6a). Meanwhile, the specific capacitance of NSGBC//NSGBC-I is 41.1 and 20.6 F/g at current density of 1 and 5 A g<sup>-1</sup>, respectively, and the capacitance retention is 50.1%, which is lower than the level of NSGBC//NSGBC-A (its capacitance retention based on current density of 1 and 5 A g<sup>-1</sup> is 65.9%). The inferior rate performance of NSGBC//NSGBC-I is mainly attributed to the large ions size of ionic liquid (EMIM<sup>+</sup> is 0.43 nm and TFSI<sup>-</sup> is 0.29 nm) [77], which may result in a high charge transfer resistance. In response to the above inference, the EIS test was executed and the result is shown in Fig. S15. Similar to NSGBC//NSGBC-A, the EIS plot of NSGBC//NSGBC-I can still be fitted by ZSimpWin based on the same equivalent circuit, and the fitting results are summarized in Table S3. Obviously, the R<sub>ct</sub> of NSGBC//NSGBC-I (19.50 Ω) is much larger than that of NSGBC//NSGBC-A (0.73 Ω) due to the large ions size of EMIM TFSI. Despite this, NSGBC//NSGBC-I exhibits a very exciting energy density (61.6 Wh kg<sup>-1</sup> at 300 W kg<sup>-1</sup>, Fig. 6b), and the value is better than many reports about carbon-based symmetric supercapacitors in ionic liquid electrolyte, e.g. many BDCs (elm samara [51], bamboo [25], paper pulp mill sludge [76] and cornstalk [56]), graphene [78], commercial activated carbon [79], metal-organic framework derived carbon [80] and activated carbon/carbon nanotube composites [81]. Furthermore, the energy density of NSGBC//NSGBC-I (25.6 Wh kg<sup>-1</sup> at 7561 W kg<sup>-1</sup>) is still meaningful larger than that of NSGBC//NSGBC-A (13.1 Wh kg<sup>-1</sup> at 4474 W kg<sup>-1</sup>) at a current density of 5 A g<sup>-1</sup>, suggesting the superiority of ionic liquid applied to supercapacitors.

The NSGBC//NSGBC-I also exhibits a good cycling stability with 91.5% retention of initial specific capacitance after 5000 cycles at 2 A g<sup>-1</sup> (Fig. 6c), and the GCD curve after the cycle still displays the isosceles triangle-like shape (inset of Fig. 6c), which intuitively shows that NSGBC//NSGBC-I still has good capacitive performance after a long cycle. In addition, the fitted parameters of the EIS plot after cycle (Table S4) indicate that the capacitance attenuation of NSGBC//NSGBC-I is still mainly due to the increase in contact resistance between NSGBC and the current collector. Fig. 6d provides a comprehensive comparison of NSGBC//NSGBC-I with carbon-based symmetric supercapacitors with ionic liquid electrolyte in previously reported, and the results show that NSGBC//NSGBC-I is superior in terms of energy density, specific capacitance and cycle stability (especially compared with [79] and [82]), but it is ordinary in terms of power density and rate performance. Furthermore, in reports [51,83], these carbon materials have outstanding rate performance and power density owing to their hierarchical porous structures. As such, this finding points a way to further improve the capacitive performance of NSGBC.

#### 4. Conclusions

In summary, a unique biomass derived carbon NSGBC has been successfully prepared by a facile method with low-cost bamboo fiber as precursors. The characterization results are consistent with the experimental design: i) NSGBC possesses a large S<sub>BET</sub>, a suitable graphitization degree and excellent conductivity due to the additional activation and graphitization catalysis of K<sub>3</sub>Fe(CN)<sub>6</sub>; ii) NSGBC displays a good wettability to the electrolyte owing to the heteroatoms doping derived from thiourea; iii) especially, NSGBC also displays a unique sheet-like microstructure originated from the layer stripping of gas produced by thiourea pyrolysis. Based on the above physical-chemical and microstructure features, the NSGBC exhibits high specific capacitance and acceptable rate

capability. Simultaneously, NSGBC-based symmetric supercapacitors with aqueous electrolyte or ionic liquid electrolyte all possess outstanding energy density and excellent cycle stability. These exciting results indicate that the synthetic strategy of this study is expected to bring new ideas to the preparation of biomass derived carbon with excellent electrochemical performance.

#### Acknowledgements

This work was financially supported by the National Natural Science Foundation of China (Grant No.2127318 and No.21621091), China Postdoctoral Science Foundation (Grant No. 2018M642571) and National Found for Fostering Talents of Basic Science (J1310024).

#### Appendix A. Supplementary data

Supplementary data to this article can be found online at <https://doi.org/10.1016/j.electacta.2019.135348>.

#### References

- [1] A.K. Mohanty, S. Vivekanandhan, J.M. Pin, M. Misra, Composites from renewable and sustainable resources: challenges and innovations, *Science* 362 (2018) 536–542.
- [2] L. Li, Q. Zhong, N.D. Kim, G. Ruan, Y. Yang, C. Gao, H. Fei, Y. Li, Y. Ji, J.M. Tour, Nitrogen-doped carbonized cotton for highly flexible supercapacitors, *Carbon* 105 (2016) 260–267.
- [3] L.F. Zhu, F. Shen, R.L. Smith Jr., L.L. Yan, L.Y. Li, X.H. Qi, Black liquor-derived porous carbons from rice straw for high-performance supercapacitors, *Chem. Eng. J.* 316 (2017) 770–777.
- [4] Y.S. Yun, S.Y. Cho, J.Y. Shim, B.H. Kim, S.J. Chang, S.J. Baek, et al., Microporous carbon nanoplates from regenerated silk proteins for supercapacitors, *Adv. Mater.* 25 (2013) 1993–1998.
- [5] H. Feng, H. Hu, H. Dong, Y. Xiao, Y. Cai, B. Lei, et al., Hierarchical structured porous carbons from bagasse wastes: a simple and efficient synthesis route and its improved electrochemical properties for high-performance supercapacitors, *J. Power Sources* 302 (2016) 164–173.
- [6] T. Bharathidasan, T.N. Narayanan, S. Sathyanarayanan, S.S. Sreejakumari, Above 170° water contact angle and oleophobicity of fluorinated graphene oxide based transparent polymeric films, *Carbon* 84 (2014) 207–213.
- [7] X.C. Dong, J. Chen, Y.W. Ma, J. Wang, M.B. Chan-Park, X.M. Liu, et al., Superhydrophobic and superoleophilic hybrid foam of graphene and carbon nanotube for selective removal of oils or organic solvents from the surface of water, *Chem. Commun.* 48 (2012) 10660–10662.
- [8] Y.J. Li, G.L. Wang, T. Wei, Z.J. Fan, P. Yan, Nitrogen and sulfur co-doped porous carbon nanosheets derived from willow catkin for supercapacitors, *Nano Energy* 19 (2016) 165–175.
- [9] F.L. Cheng, W. Liu, Y. Zhang, H.L. Wang, S. Liu, E.C. Hao, S.P. Zhao, H.Z. Yang, Squid inks- derived nanocarbons with unique “shell@pearls” structure for high performance supercapacitors, *J. Power Sources* 354 (2017) 116–123.
- [10] J. Niu, R. Shao, J.J. Liang, M.L. Dou, Z.L. Li, Y.Q. Huang, F. Wang, Biomass-derived mesopore-dominant porous carbons with large specific surface area and high defect density as high performance electrode materials for Li-ion batteries and supercapacitors, *Nano Energy* 36 (2017) 322–330.
- [11] Z.P. Zhang, X.J. Gao, M.L. Dou, J. Ji, F. Wang, Fe-N<sub>x</sub> moiety-modified hierarchically porous carbons derived from porphyrin for highly effective oxygen reduction reaction, *J. Mater. Chem. A* 5 (2017) 1526–1532.
- [12] Y.F. Deng, Y. Xie, K.X. Zou, X.L. Ji, Review on recent advances in nitrogen-doped carbons: preparations and applications in supercapacitors, *J. Mater. Chem. A* 4 (2016) 1144–1173.
- [13] J.P. Paraknowitsch, A. Thomas, Doping carbons beyond nitrogen: an overview of advanced heteroatom doped carbons with boron, sulphur and phosphorus for energy applications, *Energy Environ. Sci.* 6 (2013) 2839–2855.
- [14] W. Kicinski, M. Szala, M. Bystrzejewski, Sulfur-doped porous carbons: synthesis and applications, *Carbon* 68 (2014) 1–32.
- [15] X. Yu, S.K. Park, S.H. Yeon, H.S. Park, Three-dimensional, sulfur-incorporated graphene aerogels for the enhanced performances of pseudocapacitive electrodes, *J. Power Sources* 278 (2015) 484–489.
- [16] K. Gopalsamy, J. Balamurugan, T.D. Thanh, N.H. Kim, J.H. Lee, Fabrication of nitrogen and sulfur co-doped graphene nanoribbons with porous architecture for high-performance supercapacitors, *Chem. Eng. J.* 312 (2017) 180–190.
- [17] W.J. Zhang, Z.T. Chen, X.L. Guo, K. Jin, Y.X. Wang, L. Li, et al., N/S co-doped three-dimensional graphene hydrogel for high performance supercapacitor, *Electrochim. Acta* 278 (2018) 51–60.
- [18] S. Wang, E. Iyyamperumal, A. Roy, Y. Xue, D. Yu, L. Dai, Vertically aligned BCN nanotubes as efficient metal-free electrocatalysts for the oxygen reduction reaction: a synergetic effect by Co-doping with boron and nitrogen, *Angew.*

- Chem. Int. Ed. 50 (2011) 11756–11760.
- [19] H. Lei, Y.H. Wang, J.C. Huo, Porous graphitic carbon materials prepared from cornstarch with the assistance of microwave irradiation, *Microporous Mesoporous Mater.* 210 (2015) 39–45.
- [20] T.J. Fu, J. Lv, Z.H. Li, Effect of carbon porosity and cobalt particle size on the catalytic performance of carbon supported cobalt fischer-tropsch catalysts, *Ind. Eng. Chem. Res.* 53 (2014) 1342–1350.
- [21] N. Kasahara, S. Shiraishi, A. Oya, Heterogeneous graphitization of thin carbon fiber derived from phenol-formaldehyde resin, *Carbon* 41 (2003) 1654–1656.
- [22] M. Sevilla, C. Sanchis, T. Valdes-Solis, E. Morallon, A.B. Fuertes, Direct synthesis of graphitic carbon nanostructures from saccharides and their use as electrocatalytic supports, *Carbon* 46 (2008) 931–939.
- [23] A. Oya, H. Marsh, Phenomena of catalytic graphitization, *J. Mater. Sci.* 17 (1982) 309–322.
- [24] M. Demir, Z. Kahveci, B. Aksoy, N.K.R. Palapati, A. Subramanian, H.T. Cullinan, et al., Graphitic biocarbon from metal-catalyzed hydrothermal carbonization of lignin, *Ind. Eng. Chem. Res.* 54 (2015) 10731–10739.
- [25] Y. Gong, D. Li, C. Luo, Q. Fu, C. Pan, Highly porous graphitic biomass carbon as advanced electrode materials for supercapacitors, *Green Chem.* 19 (2017) 4132–4140.
- [26] A.C. Ferrari, J.C. Meyer, V. Scardaci, C. Casiraghi, M. Lazzeri, F. Mauri, et al., Raman spectrum of graphene and graphene layers, *Phys. Rev. Lett.* 97 (2006) 187401.
- [27] B. Wang, J.H. Qiu, H.X. Feng, E. Sakai, Preparation of graphene oxide/polypropylene/multi-walled carbon nanotube composite and its application in supercapacitors, *Electrochim. Acta* 151 (2015) 230–239.
- [28] C. Cheng, S. Li, A. Thomas, N.A. Kotov, R. Haag, Functional graphene nano-materials based architectures: biointeractions, fabrications, and emerging biological applications, *Chem. Rev.* 117 (2017) 1826–1914.
- [29] M.Y. Yan, F.C. Wang, C.H. Han, X.Y. Ma, X. Xu, Q.Y. An, et al., Nanowire templated semihollow bicontinuous graphene scrolls: designed construction, mechanism, and enhanced energy storage performance, *J. Am. Chem. Soc.* 135 (2013) 18176–18182.
- [30] H. Wang, Z. Xu, A. Kohandehghan, Z. Li, K. Cui, X. Tan, et al., Interconnected carbon nanosheets derived from hemp for ultrafast supercapacitors with high energy, *ACS Nano* 7 (2013) 5131–5141.
- [31] D.W. Wang, F. Li, M. Liu, G.Q. Lu, H.M. Cheng, Mesopore-aspect-ratio dependence of ion transport in rod-type ordered mesoporous carbon, *J. Phys. Chem. C* 112 (2008) 9950–9955.
- [32] L. Sun, C.G. Tian, M.T. Li, X.Y. Meng, L. Wang, R.H. Wang, et al., From coconut shell to porous graphene-like nanosheets for high-power supercapacitors, *J. Mater. Chem. A* 1 (2013) 6462–6470.
- [33] Z.P. Wang, H. Ogata, S. Morimoto, J. Ortiz-Medina, M. Fujishige, K. Takeuchi, et al., Nanocarbons from rice husk by microwave plasma irradiation: from graphene and carbon nanotubes to graphenated carbon nanotube hybrids, *Carbon* 94 (2015) 479–484.
- [34] Y.Z. Su, Y. Zhang, X.D. Zhuang, S. Li, D.Q. Wu, F. Zhang, et al., Low-temperature synthesis of nitrogen/sulfur co-doped three-dimensional graphene frameworks as efficient metal-free electrocatalyst for oxygen reduction reaction, *Carbon* 62 (2013) 296–301.
- [35] R. Ramya, R. Sivasubramanian, M.V. Sangaranarayanan, Conducting polymers-based electrochemical supercapacitors—Progress and prospects, *Electrochim. Acta* 101 (2013) 109–129.
- [36] S. Maldonado, S. Morin, K.J. Stevenson, Structure, composition, and chemical reactivity of carbon nanotubes by selective nitrogen doping, *Carbon* 44 (2006) 1429–1437.
- [37] R.R. Gaddam, D.F. Yang, R. Narayan, K. Raju, N.A. Kumar, X.S. Zhao, Biomass derived carbon nanoparticle as anodes for high performance sodium and lithium ion batteries, *Nano Energy* 26 (2016) 346–352.
- [38] J. Gamby, P.L. Taberna, P. Simon, J.F. Fauvarque, M. Chesneau, Studies and characterisations of various activated carbons used for carbon/carbon supercapacitors, *J. Power Sources* 101 (2001) 109–116.
- [39] B. Wang, J.H. Qiu, H.X. Feng, E. Sakai, T. Komiyama, KOH-activated nitrogen doped porous carbon nanowires with superior performance in supercapacitors, *Electrochim. Acta* 190 (2016) 229–239.
- [40] B. Wang, L.L. Ji, Y.L. Yu, N.X. Wang, J. Wang, J.B. Zhao, A simple and universal method for preparing N, S co-doped biomass derived carbon with superior performance in supercapacitors, *Electrochim. Acta* 309 (2019) 34–43.
- [41] Y. Qiao, M.Y. Ma, Y. Liu, S. Li, Z.S. Lu, H.Y. Yue, et al., First-principles and experimental study of nitrogen/sulfur co-doped carbon nanosheets as anodes for rechargeable sodium ion batteries, *J. Mater. Chem. A* 4 (2016) 15565–15574.
- [42] Q.X. Lai, Y.X. Zhao, Y.Y. Liang, J.P. He, J.H. Chen, In situ confinement pyrolysis transformation of ZIF-8 to nitrogen-enriched meso-microporous carbon frameworks for oxygen reduction, *Adv. Funct. Mater.* 26 (2016) 8334–8344.
- [43] X. Wang, G. Sun, P. Routh, D.-H. Kim, W. Huang, P. Chen, Heteroatom-doped graphene materials: syntheses, properties and applications, *Chem. Soc. Rev.* 43 (2014) 7067–7098.
- [44] M. Wahid, G. Parte, D. Phase, S. Ogale, Yogurt: a novel precursor for heavily nitrogen doped supercapacitor carbon, *J. Mater. Chem. A* 3 (2015) 1208–1215.
- [45] D. Liu, C. Zeng, D. Qu, H. Tang, Y. Li, B.-L. Su, D. Qu, Highly efficient synthesis of ordered nitrogen-doped mesoporous carbons with tunable properties and its application in high performance supercapacitors, *J. Power Sources* 321 (2016) 143–154.
- [46] X. Yu, H.S. Park, Sulfur-incorporated, porous graphene films for high performance flexible electrochemical capacitors, *Carbon* 77 (2014) 59–65.
- [47] T.J. Bandoz, T.Z. Ren, Porous carbon modified with sulfur in energy related applications, *Carbon* 118 (2017) 561–577.
- [48] H. Chen, M. Zhou, Z. Wang, S.Y. Zhao, S.Y. Guan, Rich nitrogen-doped ordered mesoporous phenolic resin-based carbon for supercapacitors, *Electrochim. Acta* 148 (2014) 187–194.
- [49] T.J. Bandoz, T.Z. Ren, Porous carbon modified with sulfur in energy related applications, *Carbon* 118 (2017) 561–577.
- [50] Y.Y. Lv, F. Zhang, Y.Q. Dou, Y.P. Zhai, J.X. Wang, H.J. Liu, Y.Y. Xia, B. Tu, D.Y. Zhao, A comprehensive study on KOH activation of ordered mesoporous carbons and their supercapacitor application, *J. Mater. Chem.* 22 (2012) 93–99.
- [51] C. Chen, D.F. Yu, G.Y. Zhao, B.S. Du, W. Tang, L. Sun, et al., Three-dimensional scaffolding framework of porous carbon nanosheets derived from plant wastes for high-performance supercapacitors, *Nanomater. Energy* 27 (2016) 377–389.
- [52] Y. Tan, C. Xu, G. Chen, Z. Liu, M. Ma, Q. Xie, N. Zheng, S. Yao, Synthesis of ultrathin nitrogen-doped graphitic carbon nanocages as advanced electrode materials for supercapacitor, *ACS Appl. Mater. Interfaces* 5 (2013) 2241–2248.
- [53] K. Jayaramulu, D.P. Dubal, B. Nagar, V. Ranc, O. Tomanec, M. Petr, et al., Ultrathin hierarchical porous carbon nanosheets for high-performance supercapacitors and redox electrolyte energy storage, *Adv. Mater.* 30 (2018) 1705789.
- [54] S. Gao, X. Li, L. Li, X. Wei, A versatile biomass derived carbon material for oxygen reduction reaction, supercapacitors and oil/water separation, *Nano Energy* 33 (2017) 334–342.
- [55] C. Young, R.R. Salunkhe, J. Tang, C.C. Hu, M. Shahabuddin, E. Yanmaz, et al., Zeolitic imidazolate framework (ZIF-8) derived nanoporous carbon: the effect of carbonization temperature on the supercapacitor performance in an aqueous electrolyte, *Phys. Chem. Chem. Phys.* 18 (2016) 29308–29315.
- [56] L. Wang, G. Mu, C. Tian, L. Sun, W. Zhou, P. Yu, et al., Porous graphitic carbon nanosheets derived from cornstarch biomass for advanced supercapacitors, *ChemSusChem* 6 (2013) 880–889.
- [57] Y. Jiang, J. Yan, X. Wu, D. Shan, Q. Zhou, L. Jiang, et al., Facile synthesis of carbon nanofibers-bridged porous carbon nanosheets for high-performance supercapacitors, *J. Power Sources* 307 (2016) 190–198.
- [58] B. Liu, Y. Liu, H. Chen, M. Yang, H. Li, Oxygen and nitrogen co-doped porous carbon nanosheets derived from Perilla frutescens for high volumetric performance supercapacitors, *J. Power Sources* 341 (2017) 309–317.
- [59] P. Cheng, T. Li, H. Yu, L. Zhi, Z. Liu, Z. Lei, Biomass-derived carbon fiber aerogel as a binder-free electrode for high-rate supercapacitors, *J. Phys. Chem. C* 120 (2016) 2079–2086.
- [60] G. Zhang, L. Wang, Y. Hao, X. Jin, Y. Xu, Y. Kuang, et al., Unconventional carbon: alkaline dehalogenation of polymers yields N-doped carbon electrode for high-performance capacitive energy storage, *Adv. Funct. Mater.* 26 (2016) 3340–3348.
- [61] W.M. Qiao, S.H. Yoon, I. Mochida, KOH activation of needle coke to develop activated carbons for high-performance EDLC, *Energy Fuel.* 20 (2006) 1680–1684.
- [62] C.C. Xiang, M. Li, M.J. Zhi, A. Manivannan, N.Q. Wu, Reduced graphene oxide/titanium dioxide composites for supercapacitor electrodes: shape and coupling effects, *J. Mater. Chem.* 22 (2012) 19161–19167.
- [63] X.J. Wei, Y.B. Li, S.Y. Gao, Biomass-derived interconnected carbon nanorings electrochemical capacitors with high performance in both strongly acidic and alkaline electrolytes, *J. Mater. Chem. A* 5 (2017) 181–188.
- [64] T.W. Cai, M. Zhou, D.Y. Ren, G.S. Han, S.Y. Guan, Highly ordered mesoporous phenol-formaldehyde carbon as supercapacitor electrode material, *J. Power Sources* 231 (2013) 197–202.
- [65] J. Diana, H. Francisco, M.A. Gilarranz, R. Encarnacion, Grape seed carbons for studying the influence of texture on supercapacitor behaviour in aqueous electrolytes, *Carbon* 71 (2014) 127–138.
- [66] Y. Xu, Y.B. Kang, H.S. Park, Sulfur and phosphorus co-doping of hierarchically porous graphene aerogels for enhancing supercapacitor performance, *Carbon* 101 (2016) 49–56.
- [67] C.L. Long, X. Chen, L.L. Jiang, L.J. Zhi, Z.J. Fan, Porous layer-stacking carbon derived from in-built template in biomass for high volumetric performance supercapacitors, *Nano Energy* 12 (2015) 141–151.
- [68] D.D. Shan, J. Yang, W. Liu, J. Yan, Z.J. Fan, Biomass-derived three-dimensional honeycomblike hierarchical structured carbon for ultrahigh energy density asymmetric supercapacitors, *J. Mater. Chem. A* 4 (2016) 13589–13602.
- [69] P. Staiti, A. Arenillas, F. Lufrano, J.A. Menéndez, High energy ultracapacitor based on carbon xerogel electrodes and sodium sulfate electrolyte, *J. Power Sources* 214 (2012) 137–141.
- [70] Q. Gao, L. Demarconay, E. Raymundo-Piñero, F. Béguin, Exploring the large voltage range of carbon/carbon supercapacitors in aqueous lithium sulfate electrolyte, *Energy Environ. Sci.* 5 (2012) 9611–9617.
- [71] M.P. Bichat, E.R. Pinero, F. Béguin, High voltage supercapacitor built with seaweed carbons in neutral aqueous electrolyte, *Carbon* 48 (2010) 4351.
- [72] Q. Wang, J. Yan, Z. Fan, Nitrogen-doped sandwich-like porous carbon nanosheets for high volumetric performance supercapacitors, *Electrochim. Acta* 146 (2014) 548–555.
- [73] K. Gopalsamy, J. Balamurugan, T.D. Thanh, N.H. Kim, J.H. Lee, Fabrication of nitrogen and sulfur co-doped graphene nanoribbons with porous architecture for high-performance supercapacitors, *Chem. Eng. J.* 312 (2017) 180–190.
- [74] Q. Wang, J. Yan, T. Wei, J. Feng, Y. Ren, Z. Fan, et al., Two-dimensional

- mesoporous carbon sheet-like framework material for high-rate supercapacitors, *Carbon* 60 (2013) 481–487.
- [75] S. Zhang, X.Z. Shi, D. Moszyński, T. Tang, P.K. Chu, X.C. Chen, et al., Hierarchical porous carbon materials from nanosized metal-organic complex for high-performance symmetrical supercapacitor, *Electrochim. Acta* 269 (2018) 580–589.
- [76] H.L. Wang, Z. Li, J.K. Tak, C.M.B. Holt, X.H. Tan, Z.W. Xu, et al., Supercapacitors based on carbons with tuned porosity derived from paper pulp mill sludge biowaste, *Carbon* 57 (2013) 317–328.
- [77] D. Weingarh, M. Zeiger, N. Jäckel, M. Aslan, G. Feng, V. Presser, Graphitization as a universal tool to tailor the PotentialDependent capacitance of carbon supercapacitors, *Adv. Energy Mater.* 4 (2014) 1400316.
- [78] T.Y. Kim, H.W. Lee, M. Stoller, D.R. Dreyer, C.W. Bielawski, et al., High-performance supercapacitors based on poly(ionic liquid)-modified graphene electrodes, *ACS Nano* 5 (2011) 436–442.
- [79] A. Balducci, R. Dugas, P.L. Taberna, P. Simon, D. Plée, M. Mastragostino, et al., High temperature carbon-carbon supercapacitor using ionic liquid as electrolyte, *J. Power Sources* 165 (2007) 922–927.
- [80] J. Hu, H.L. Wang, Q.M. Gao, H.L. Guo, Porous carbons prepared by using metal-organic framework as the precursor for supercapacitors, *Carbon* 48 (2010) 3599–3606.
- [81] W. Lu, R. Hartman, Nanocomposite electrodes for high-performance supercapacitors, *J. Phys. Chem. Lett.* 2 (2011) 655–660.
- [82] J. Zhou, X. Yuan, W. Xing, W.J. Si, S.P. Zhuo, Capacitive performance of mesoporous carbons derived from the citrates in ionic liquid, *Carbon* 48 (2010) 2765–2772.
- [83] S. Zhang, X.Z. Shi, D. Moszyński, T. Tang, P.K. Chu, X.C. Chen, et al., Hierarchical porous carbon materials from nanosized metal-organic complex for high-performance symmetrical supercapacitor, *Electrochim. Acta* 269 (2018) 580–589.